Scaling control by using ultrasonic guided waves

Nihad Kamar, Hervé Muhr, Marie Le Page Mostefa, Pierre-Olivier Jost

Scaling control by using ultrasonic guided waves

*Nihad KAMAR**, *University of Lorraine/CNRS-LRGP, Nancy/France; Marie LE PAGE MOSTEFA, University of Lorraine/CNRS-LRGP, Nancy/France; Hervé MUHR, University of Lorraine/CNRS-LRGP, Nancy/France; Pierre-Olivier JOST, Sofchem, Rueil Malmaison/France*

**Corresponding author*

Highlights

- Design of a heat exchanger pilot to study scaling.
- Identification of the nature of the deposited scale using PHREEQC simulations.
- Quantification of the quantity deposited experimentally.
- Analysis of the distribution of scale on the heat exchanger by 3D microscopy.
- Evaluation of the impact of the ultrasonic treatment on scale formation.

Abstract

Scaling of equipment is a major concern in industry. The fouling of heat exchanger surfaces leads to performance losses through a decrease in the overall heat exchange coefficient. Control methods exist but are costly and have a strong environmental impact. Thus, the use of physical treatments proves to be very promising, because the action is done on the surface which is clogged, and not on the solution.

The present study shows the influence of ultrasonic guide waves on the crystallization of calcium carbonate inside a gasketed plate heat exchanger from a water with scaling power. An experimental pilot was set up to study the scaling phenomenon and to evaluate the deposit quantitatively and qualitatively. Several operating parameters such as flow rate, duration and temperature were varied experimentally in order to identify their influence on the scale deposition in the heat exchanger.

Four types of experiments lasting three days will be presented in this paper to show experimentally the influence of ultrasound generated by a transducer 35-50 kHz on the formation of scale. The amount of solid deposited, the polymorphism of the formed crystals, the number, size and size distribution of the particles will be analyzed.

The main focus is on the amount of scale deposited on the exchanger plates, estimated in grams/per day/surface unit from the determination of carbonates by TOC analyzer and Ca^{2+}, Mg^{2+} by ICP-OES after dissolving the scale in 2% nitric acid. The identification of the physico-chemical nature of the scale is performed by RAMAN spectroscopy and the surface topography is obtained by scanning electron microscope (SEM). In addition, the elemental composition of the scale was determined by SEM EDXS probe.

Disassembly of the exchanger allows access to the distribution of the scale on the plates, and thus justifies the choice of the location of the 35-50 kHz transducer. It is also possible to estimate the thickness of the scale by 3D microscopy, and to ensure the absence of microcrystals in the pores of the plate by analyzing the surface roughness.

Subsequently, a thermodynamic prediction was made through geochemical modelling using the Phreeqc software. The results obtained were compared to experimental measurements, with or without the presence of the 35-50 kHz transducer. This will allow the evaluation of the effect of ultrasonic guided waves for the prevention of calcareous deposits.

The presence of a single medium power transducer allows a 76 % reduction in mineral scale deposition within a plate and gasket heat exchanger.

Graphic abstract

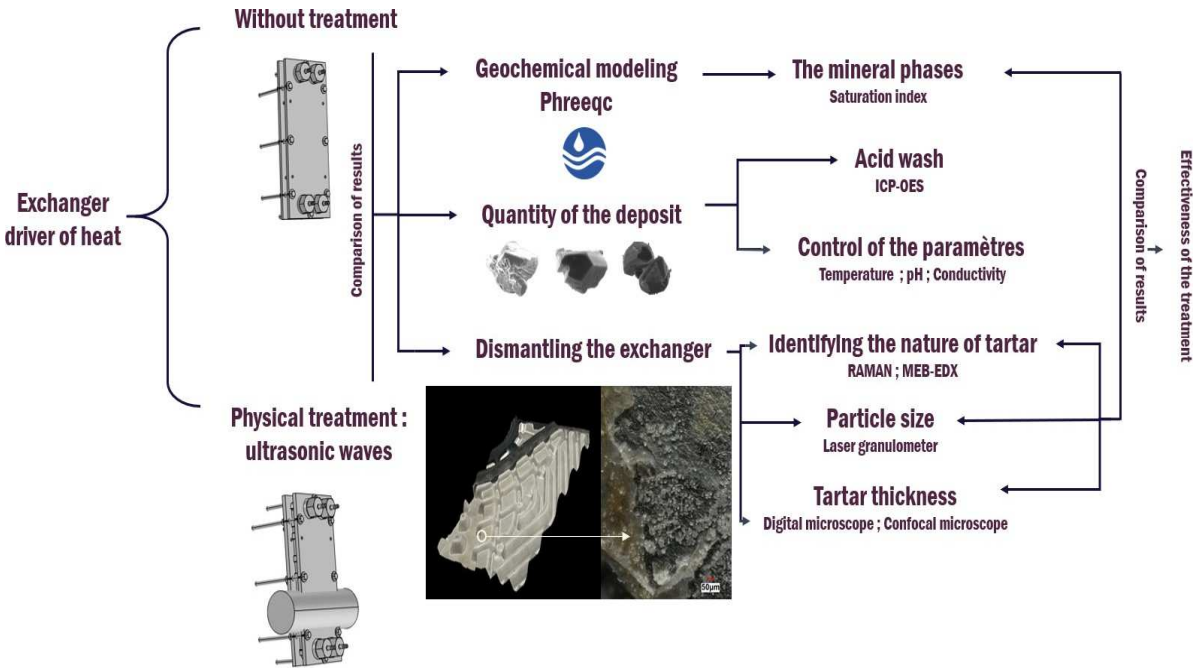

Key words

Scaling, Heat exchanger, Ultrasounds, PHREEQC simulation, Crystallization, Calcium carbonate.

Nomenclature

Symbol	Name	Dimension
I. Abbreviations		
$CaCO_3$	Calcium carbonate	
$CaMg(CO_3)_2$	Dolimite	
$Ca(NO_3)_2$	Calcium nitrate	
CO_2	Carbon dioxide	
EDXS	Energy Dispersive X-ray Spectroscopy	
HCO_3^-	Bicarbonate	
ICP-OES	Inductively Coupled Plasma Atomic Emission Spectroscopy	
Nu	Nusselts number	
PEEK	Polyetheretherketone seals	
PFA	Perfluoroalkoxy	
pH	Hydrogen potential	
ppm	Part per million	
Pr	Prandtl number	
Re	Reynolds number	
rpm	Rotations per minute	

SEM	Scanning Electron Microscope	
TOC	Total Organic Carbon	
II.	***Geometric dimensions, amounts, concentrations***	
α	Corrugation angle	**-**
C_i	Molar concentration of species i	$\mathbf{N.L^{-3}}$
D_H	Hydraulic diameter	**L**
L	Plate length	**L**
m_i	Mass of species i	**M**
n_i	Number of moles of species i	**N**
P	Perimeter	**L**
SI	Saturation index	**-**
V	Volume	$\mathbf{L^3}$
z_i	Ionic charge	**-**
III.	***Physical properties***	
γ	Coefficient activity of species i	**-**
f	Coefficient of friction	**-**
K_S	Solubility product	**-**
M_i	Molar mass of species i	$\mathbf{M.N^{-1}}$
ρ	Density	$\mathbf{M.L^{-3}}$
T	Temperature	**Θ**
X	Conductivity	$\mathbf{M.L.T^{-3}.\Theta^{-1}}$
IV.	***Time, velocities, and flow rates***	
ΔP	Pressure drop	$\mathbf{M.L^{-1}.T^{-2}}$
u	Velocity	$\mathbf{L.T^{-1}}$
V.	***Index***	
i	Initial	
f	Final	
$tank$	Storage tank of cold water	

Table of Contents

Introduction

Gasketed plate heat exchangers are used in a wide variety of applications, to transfer thermal energy, preheat or cool a liquid or refrigerate a process, serve as a condenser or evaporator... (Eldeeb et al., 2016). The industries resorting to the use of plate and gasket heat exchangers are numerous and varied such as food and beverage, pharmaceutical, biotechnology, chemical, petrochemical and power generation systems. They are often more economical than shell-and-tube heat exchangers and easier to install and maintain. Currently, there are many manufacturers of heat exchangers on the European market, such as: Alfa Laval (Grenoble, Nevers and Chalon- sur-Saône), API Heat Transfer (Germany, China, USA and England), Barriquand (France), CIAT (France), Danfoss (Denmark), Güntner (Germany), Hamon (Belgium), Hisaka (Asia), HVAC (Japan, China), Kelvion (Germany), Lennox (France), Mersen (France), Profroid (USA, France), Sondex (Denmark, France), SPX (USA), Swep (Sweden), ThermoKey (Italy), Tranter (USA, Tranter is now the world's largest supplier of exchangers), Wesper (France).

Scaling of heat exchangers in general is a major problem that results in the formation of $CaCO_3$ crystals on the surface of the plates, which leads to a decrease in the overall exchange coefficient and causes pressure losses.

Chemical cleaning processes are costly and polluting, requiring the shutdown of the installation and sometimes the dismantling of the equipment, which leads to high costs and operating losses. Solutions to limit the scaling of exchanger surfaces consist mainly of the use of phosphate- based chemical inhibitors (polyphosphates; phosphonates; phosphonocarbonates; polymers, copolymers and terpolymers; polypeptides and polysaccharides (easily biodegradable)). The use of these inhibitors increases the concentration factor by extending the solubility limit of the scaling salts, but also by allowing the salts to precipitate in a non-scaling form if the solubility limit is locally exceeded.

The purpose of this work is to study the effects of ultrasonic guided waves generated by a conventional transducer on the precipitation of calcium carbonate inside a plate heat exchanger.

When ultrasound is emitted into a liquid, four phenomena can occur:

- Heating of the liquid due to acoustic energy;
- Acoustic current due to the creation of a momentum gradient;

- Cavitation phenomenon that appears due to microbubbles of vapor in the liquid, which are responsible for a micro-agitation at the wall;
- Nebulization or acoustic fountain on the surface (De et al., 2012).

Habidi et al (2020) have shown that ultrasonic guided waves at applied frequencies of 20-45 kHz can limit biofouling of ship hulls.

In addition, Taylor and Richardson (1982) demonstrated the effectiveness of ultrasonic treatment to inhibit fouling in heat exchangers and pipes by applying a few short pulses of high- power ultrasonic waves.

Under conditions suitable for artificial fouling, Mathieu et al (n.d.) demonstrate the feasibility of low frequency, low intensity ultrasonic treatment on fouling of a plate heat exchanger on a laboratory scale.

Our study is based on the monitoring over time of the temperature, the concentration of Ca^{2+}, Mg^{2+}, carbonates, the flow rate, the induction time of calcium carbonate precipitation, the size distribution of the crystals on the exchange surface, as well as the polymorphic forms present (calcite, aragonite, vaterite) with or without ultrasonic treatment

1 Materials and methods

1.1 Experimental device

1.1.1 Description of the experimental pilot - without ultrasound

The objective of the work carried out is to study the formation of $CaCO_3$ by raising the temperature of a natural, hard water (30 °F), within a plate heat exchanger. For this purpose, an experimental pilot was designed and developed, the operation of which is shown in figure 1.

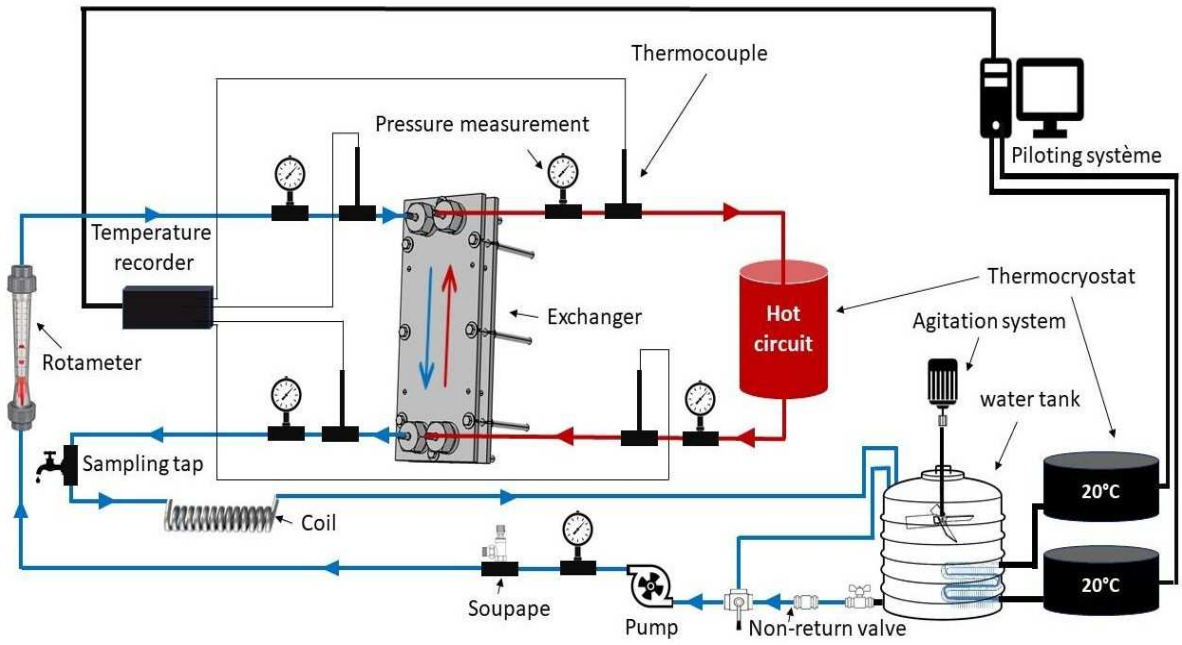

Figure 1: Description of the experimental setup without ultrasonic treatment

It consists of a heat exchanger supplied by Barriquand. It is a plate and gasket exchanger BAS*32*381*C*P11 (flow rate range 1-10 $m^3.h^{-1}$) consisting of 10 plates (five hot channels and four cold channels) in stainless steel 316 L developing an exchange surface of 0.38 m^2.

The "hot" circuit (in red) is made up of ultrapure water whose temperature is fixed at 50°C by the use of a Julabo cryo CD thermo-cryostat whose internal volume is 20 ± 0.1 L with a flow rate of 16 $L.min^{-1}$.

The "cold" circuit (in blue) consists of a tank with a maximum capacity of 300 L filled with 100 ± 2 L of natural water whose ion concentrations are presented in Table 1:

Table 1: Composition of the water on the cold side

$[Ca^{2+}]$ (mg. L^{-1})	$[Mg^{2+}]$ (mg. L^{-1})	$[CO_3^{2-}]$ (mg. L^{-1})
90 - 160	8 - 12	30 - 60

Note that the concentrations indicated in Table 1 are determined by ICP-OES analysis (*ThermoScientific ICP-OES ICAP 6300 DUO*) and TOC analysis (*METTLER TOLEDO 450TOC portable TOC analyzer*). The temperature in the tank is set at 23 ± 4 °C using two thermo-cryostats, Julabo ME thermo-cryostat filled with 8 ± 0.1 L of Kryohydre oil and Thermoscientific thermo-cryostat filled with 10 ± 0.1 L of commercial propylene glycol. The temperature inside the

tank is homogenized by a mechanical stirring system. A gear pump allows the circulation of cold water in the exchanger with a flow rate close to 0.1 m3.h^{-1}. A

pressure gauge and a safety valve are placed at the pump outlet to control the pressure. A non-return valve is installed at the pump inlet to prevent water from flowing back into the storage tank when the pump is stopped. It should be noted that the "cold" water leaving the exchanger has a relatively high temperature. It passes through a metal coil made by the company MOGRA, placed in ice, to allow an initial cooling in order to more easily maintain the temperature of 20°C in the tank. The frigories are brought by the circulation of a thermofluid (Thermocryostat Julabo and Thermoscientific) within two coils of length 4 meters placed in the tank.

Prosensor single class J thermocouples are installed at each inlet and outlet of the exchanger and are connected to a TC-08USB RS Component temperature recorder to ensure continuous monitoring of temperature and heat exchange quality during the experiment. Pressure gauges are installed at each inlet to monitor the pressure drop inside the exchanger.

Pressure gauges, valves, and PFA tubing are compatible with any water quality and are also compatible with 1%-10% nitric acid. Check valves, valves, and all fittings and adapters are Swagelok brand.

The pump used in this study is an ISMATEC gear pump, consisting of a BVP-Z motor with a potentiometer linked to an internal electronic board, which opens the possibility of controlling it remotely.

The pump head used in this study is type MI0378 (PEEK seal compatible with 10% nitric acid). The operating temperature must be between -29 °C and +177 °C and 3.5 bar (50 psi)). Initial testing is performed at a speed of 116 rpm (approximately 72 L.h^{-1}). Table 2 shows the characteristics of the model used.

Table 2: Pump head operating characteristics and associated flow rates

	Theoretical flow rate (L/h)	**Value indicated on potentiometer (-)**	**Displayed speed (rpm)**	**Pump head rotation speed (rpm)**
Min	4,4	1	60	10
Max	434	999	6000	1000

The flow rate delivered by the pump is checked regularly by potting. The volume set for this verification is 1 L, taken at the exchanger outlet.

In order to limit heat loss from the heat exchanger and to avoid the impact of ambient temperature variations, an insulating cover is manufactured by the company Floxor, mainly from glass wool and glass fabric (see figure 2).

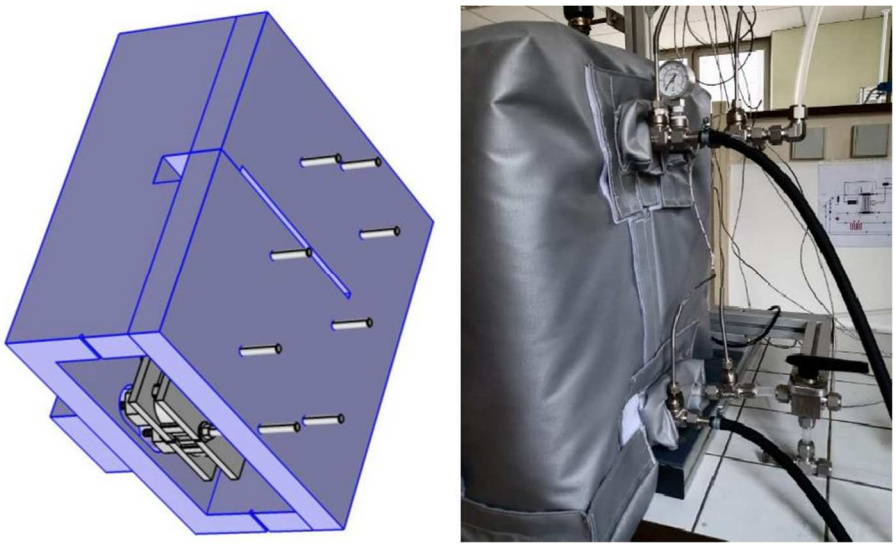

Figure 2: Design and photograph of the insulating cover of the heat exchanger

In order to determine the optimal operating conditions for the pilot, which would maximize the amount of scale deposited, two series of tests were carried out, varying the flow rate and the duration of the experiment. According to the experimental results obtained, the flow rate was set at 100 $L.h^{-1}$ (230 rpm) and the duration of the tests was set at 72 hours.

The hydrodynamic regimes are variable, turbulent in the tubes and laminar in the two compartments of the exchanger.

The pressure losses have been estimated inside the exchanger and also for the whole cold circuit, both theoretically and experimentally, where measurements have shown them to be negligible. The calculation of the pressure losses P in the installation is made by the following correlation:

$$\Delta P = 4f\frac{\rho u^2}{2}\frac{L}{D_H}$$

With :

L: plate length (m) ;

ρ: density ($kg.m^{-3}$) ;

D_H: hydraulic diameter (m) ;

u : flow velocity ($m.s^{-1}$) ;

f: the coefficient of friction, whose value depends on the corrugation angle α and the Reynolds range.

Each week, two tests are carried out, during which the temperature, conductivity, pH and ion concentrations (Ca^{2+}, Mg^{2+}, CO_3^{2-}) are monitored. The analysis of these values is used to understand the precipitation mechanism of $CaCO_3$ and to identify the different stages of this reaction.

Calcium carbonate is a salt that has an inverse solubility. Thus, when the temperature increases, the solubility of this salt decreases.

For these salts, it is in contact with the heating wall, where the temperature is maximum, that solubility is minimal. The calcium and carbonate content as well as the pH have an impact on scale formation, as does the temperature, which is a major parameter. The result is a precipitation of calcium carbonate according to the following reaction:

$$Ca^{2+}_{(aq)} + CO^{2-}_{3(aq)} \rightleftarrows CaCO_{3(s)}$$

To determine the amount of solid precipitated in the exchanger, the cold circuit must be drained and the deposit dissolved by acid leaching. The calcium and magnesium ions will then be analyzed in solution by ICP-OES and the amount deposited will be obtained by calculation.

The leaching solution is composed of 2% (vol%) Trace MetalTM Nitric Acid, Fisher Chemical brand, which is specific for trace metal analysis and is recommended for the 6000 series ICP-OES spectroscopy used in this study. 5 ± 0.01L of the leaching solution thus prepared is introduced and circulated by a peristaltic pump in the exchanger for a minimum of 2 hours to dissolve the scale deposited on the exchanger plates according to the reaction:

$$CaCO_{3(s)} + 2HNO_{3(aq)} \rightarrow Ca^{2+}_{(aq)} + CO_{2(g)} + 2NO^{-}_{3(aq)} + H_2O$$

The appearance of CO_2 bubbles begins after 4 to 6 minutes from the start of the washing

operation. At the end of each washing operation, the pH of the aqueous solution becomes 1.2 ± 0.3. Finally, the exchanger is rinsed with water up to pH = 7 to ensure that all traces of acid have been removed. At the end of this operation, the exchanger can be considered perfectly clean. This conclusion has been confirmed several times by dismantling the exchanger and visually examining the plates.

1.1.2 Description of the experimental pilot and ultrasonic system

The ultrasonic system consists of a transducer with a frequency range of 35 kHz to 50 kHz, owned by Novall, and a control unit which consists of one or more sets of dedicated electronic boards per transducer.

The card allows to regulate the output power on the output power setpoint in VA and on the input power limitation setpoint in W.

The power output depends on the transducer impedance at its resonant frequency. The model, the location of the transducer and the tightening of the mounting system can influence the output power. In our case, the transducer mounting system is tightened with a torque wrench to 0.137 Nm.

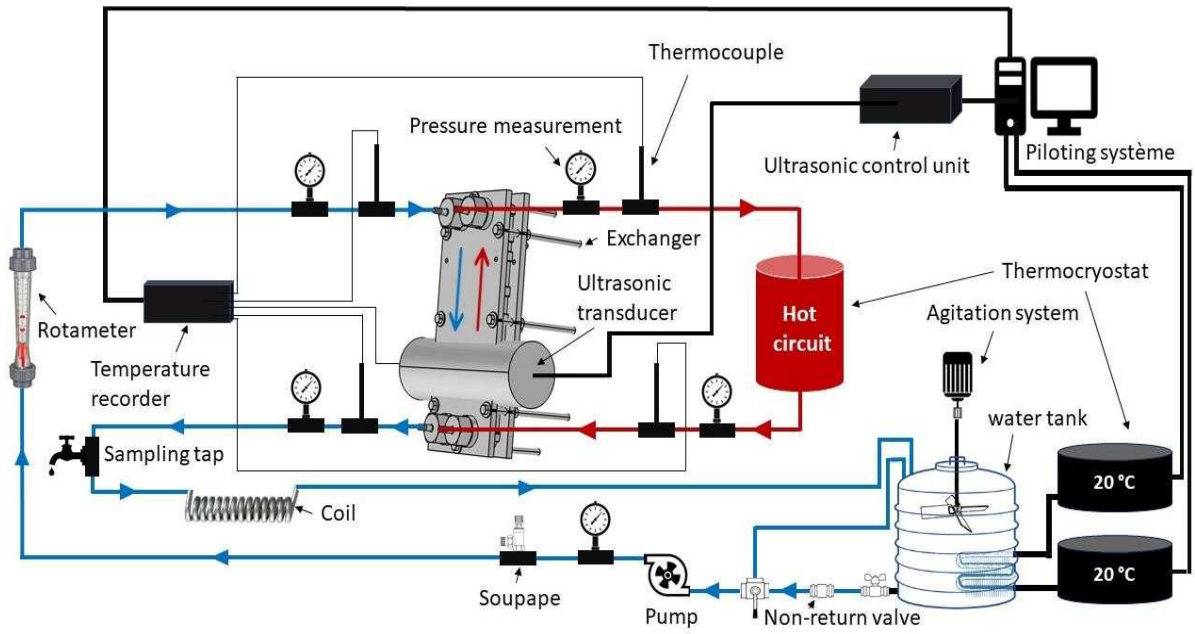

Figure 3: Description of the experimental setup in the presence of the ultrasonic transducer

1.2 Chemical analysis

1.2.1 ICP-OES spectroscopy

In order to quantify the amount of deposited scale, the deposit is dissolved in a 2% volume nitric acid solution, and the concentrations of Ca^{2+} and Mg^{2+} ions are measured by a ThermoScientific ICP-OES ICAP 6300 DUO inductively coupled plasma optical emission spectrometry instrument

1.1.1 TOC Analyzer

The measurement of total carbon is done with the portable METTLER TOLEDO 450TOC *Total Organic Carbon* (TOC) analyzer. The repeatability is ±0.05 ppbC, ± 1.0 % > 5 ppb, a resolution of 0.001 ppbC (µgC/L) and a measuring range of 0.05 to 1000 µgC/L (ppbC). Inorganic carbon is also measured by this method. With a pH measurement (Mettler Toledo), the predominant forms CO_2, HCO^{3-}, CO_3^{2-} can be determined.

1.2 Physical analysis

1.2.1 RAMAN spectroscopy

The identification of the polymorphic form of calcium carbonate is done by RAMAN spectroscopy (HORIBA Jobin Yvon XPLORA brand 020781490NE). RAMAN spectra allow the characterization of the chemical composition of the material (Deeley et al., 1991), the polymorphism (Deeley et al., 1991), as well as the electronic properties (Lepot 2011). They also provide additional information on lower frequency modes and vibrations characteristic of crystal lattices and molecular structures. This technique is non-destructive, does not require prior sample preparation and can be applied to solids, liquids or even gases (Lepot 2011).

1.2.2 Laser granulometry

Measurement of the crystal size distribution is done with a Malvern Instruments Mastersizer S laser granulometer. A laser beam passes through the measuring cell in which a suspension of particles is circulated. Each particle diffracts light at an angle depending on its size, with small particles diffracting at large angles and large particles deflecting the laser beam only slightly. A

diffraction pattern is collected and transformed into a particle size distribution using Mie or Fraunhofer theory.

1.2.3 Confocal laser scanning microscope

The Zeiss LSM 700 confocal laser scanning microscope is used in this study to measure the characteristic 3D surface roughness parameters Pa and PSa.

The optical system of confocal microscopes is based on the use of laser light passing through a confocal optical path for image formation (Bezák et al., 2013).

The confocal laser scanning microscope is well applied in the field of materials science (Monti, 2012).

In this study, a single 405 nm light source was used. Illumination is provided by a 0.5 mW solid state laser generating monochromatic light with wavelengths of 405 nm and 639 nm.

1.2.4 3D digital microscope

The Keyence VHX 3D digital microscope was used in two ways:

- To locate areas of scale accumulation through a low magnification scan of the plate (Camera VHX-702, lens VH-Z00).
- Secondly, to evaluate the thickness of the tartar thanks to the Opt-SEM (Optical Shadow Effect Mode) function. This option makes it easy to visualize height variations. This magnification is available with the VH-Z100 lens which can magnify up to 1000times.

1.2.5 Scanning electron microscope

The JEOL JSM-6490-LV scanning electron microscope was used to make high magnification observations of the crystals. It is a particularly powerful technique for the physicochemical characterization of materials (Deeley et al., 1991) and polymorphs (Deeley et al., 1991).

The preparation of the samples is restrictive. They must be dehydrated and then undergo metallization. This step is done with a plasma gold evaporator under sputtering which allows to obtain a layer of gold of 8 nm deposited on the surface, which makes the sample conductive and allows to obtain a better image afterwards. After plating, the sample is then placed on the

specimen holder.

The identification and chemical determination of the elements present are carried out using the EDXS (Energy dispersive X-ray Spectroscopy) probe.

1.3 Geochemical modelling

Monitoring the formation of scale inside the exchanger requires the ability to predict the nature of the scale formed and also to determine which mineral phase is likely to precipitate through geochemical modeling.

A prediction was made using the Phreeqc interactive 3.4.0 USGS software (Ph-Redox-Equilibrium-Calculations). This computer program based on a C programming language (Parkhurst, 1995) Version 1 Phreeqc, is capable of simulating a variety of geochemical reactions for a system including:

- mixing of waters;
- the addition of net irreversible reactions to the solution;
- the dissolution and precipitation phases to reach equilibrium with the aqueous phase;
- the effects of temperature changes.

Phreeqc interactive can calculate elemental concentrations, molarities and activities of aqueous species, pH, PE, saturation index, speciation, batch reaction and one-dimensional (1D) transport calculations involving reversible reactions, solid solution, surface complexation and ion exchange equilibria, irreversible reactions, kinetically controlled reactions, solution mixing, temperature changes and inverse modeling (Parkhurst and Appelo, 1999).

In this geochemical modeling, the system is considered to be in thermodynamic equilibrium and not all kinetic considerations are taken into account.

Geochemical modeling requires initial input constraints (Table 5). This programming language in this case consists of water chemistry analyses such as Ca^{2+}, Mg^{2+} and carbonate concentration, units of measure, temperature, dissolved gas content, pH and redox potential (Thyne, 2017).

The ionic strength I of the reaction medium is calculated according to the following relationship:

$$I = {}^{1}/_{2} \sum_{i=1}^{NC} C_i \; z_i^2$$

With,

the molar concentration of species i (mol/L);

zi: the ionic charge.

Since this study focuses on experimental tests conducted on natural waters, the ionic strength of the media does not exceed 7.9×10^{-3} mol/Kgw. Thus, a thermodynamic database such as Thermodemm (BRGM, 2017) is suitable for simulating the different equilibria establishing on the cold side, at a given temperature.

In this case, the calibration of the model based on the calculation of activity coefficients is not essential, since the concentration of minerals in drinking water is very low.

Let the precipitation reaction of the solid $A_aB_b(s)$ whose equilibrium constant is K_S:

$$aA^{x+}_{(aq)} + bB^{y-}_{(aq)} \rightleftarrows A_aB_{b(s)}$$

The saturation index SI is then obtained as follows:

$$SI = \log\left(\frac{\prod C_i\gamma_i}{K_s}\right)$$

With,

γ the activity coefficient of species i (mol/L);

Thus, when the saturation index is greater than zero, the solid ( ) can thermodynamically form, whereas if its value is negative, the solid cannot precipitate. This simulation will therefore allow us to decide whether or not crystals such as $CaCO_3$ can form, as well as their polymorphic form.

2. Results

2.1 Geochemical modelling

The typical composition of the scaling water used in the tests is shown in Table 6.

Table 6: Initial water analysis

Dimensions	***Value***
Temperature (°C)	27
pH	7,47
χ ($\mu m.cm^{-1}$)	975,8
[Ca2+] (mg. L^{-1})	88,31
[Mg2+] (mg. L^{-1})	5,90
[Carbonate] (mg. L^{-1})	58,78

The simulation results of mineral scale precipitation from scaling water are shown in the figures below:

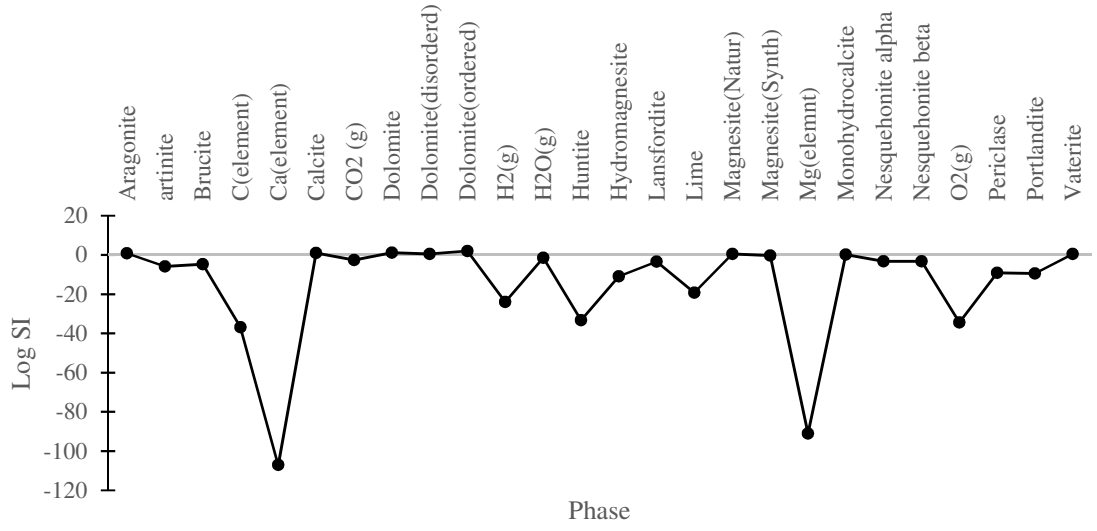

Figure 4: Potential mineral phases likely to form determined by a PHREEQC simulation from the initial composition of the water

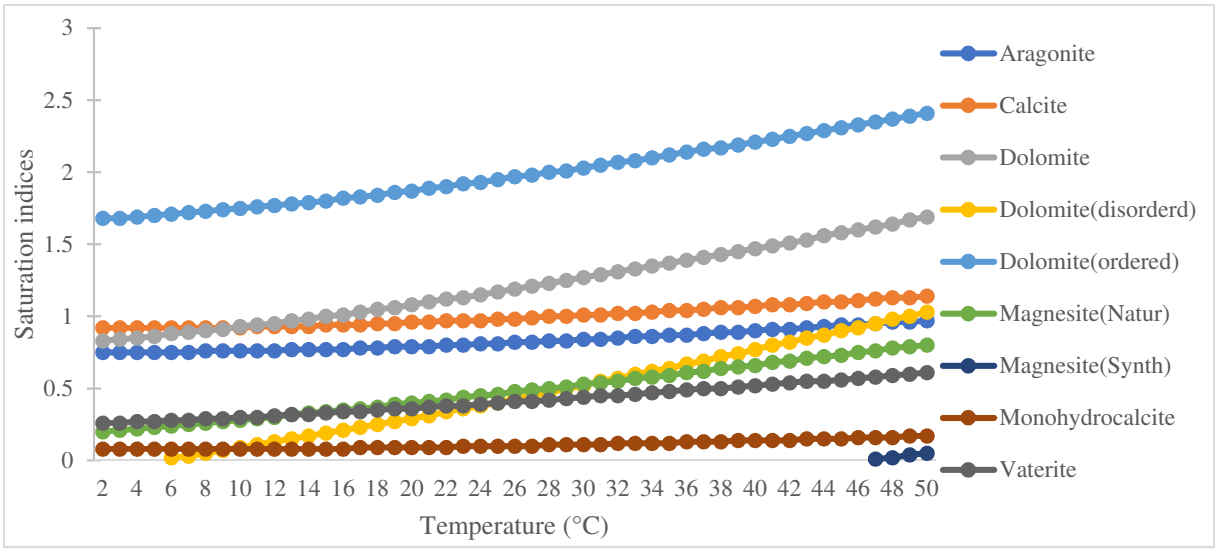

Figure 5: The variation of the saturation index of the mineral phase susceptible to precipitation as a function of temperature

The calculation of the saturation index made by Phreeqc interactive shows in the figure above, the elements hypothetically possible to precipitate. Dolomite and calcite are the elements most likely to precipitate first, and therefore most likely to form on the cold circuit exchange surface.

2.2 Distribution of scale in the exchanger

The exchanger was also dismantled to observe the distribution of scale on the cold compartment plates. This dismantling shows the presence of a non-homogeneous deposit between the plates of the same compartment. The first observations show that the scale accumulates more in the first cold compartments than in the last ones. An accumulation of scale at the inlet and outlet of the exchanger, on the cold side, is also observed.

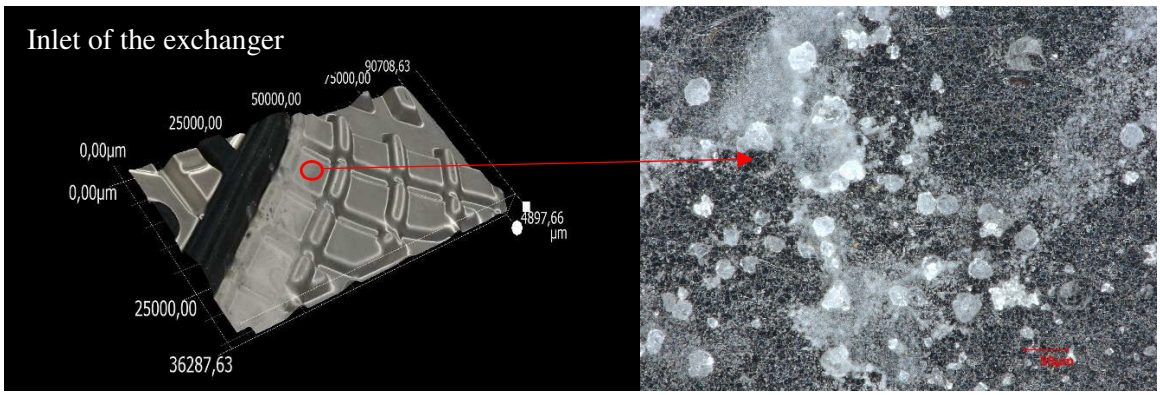

Outlet of the Exchanger

Figure 6: Scale crystals deposited on the 316L steel exchanger plate at the inlet and outlet of the first cold compartment scanned by the 3D digital microscope after 72 hours of operation, 50 °C, 100 $L.h^{-1}$

On almost all plates, the deposit is greater at the outlet than at the inlet of the cold water.

2.3 Deposit thickness

The purpose of this analysis is to make a visual diagnosis, and first of all to evaluate the thickness of the scale on an exchanger plate.

The thickness of the scale was estimated by the Keyence VHX 3D digital microscope (VH-Z100 lens) directly on a plate from the first and last cold compartment of the exchanger.

2.3.1 Without ultrasonic treatment

The analysis of the plates shows that the distribution of the scale is not homogeneous. The thickness of the scale in the first compartment can reach about 230 µm. However, in the last compartment, it does not exceed 32 µm.

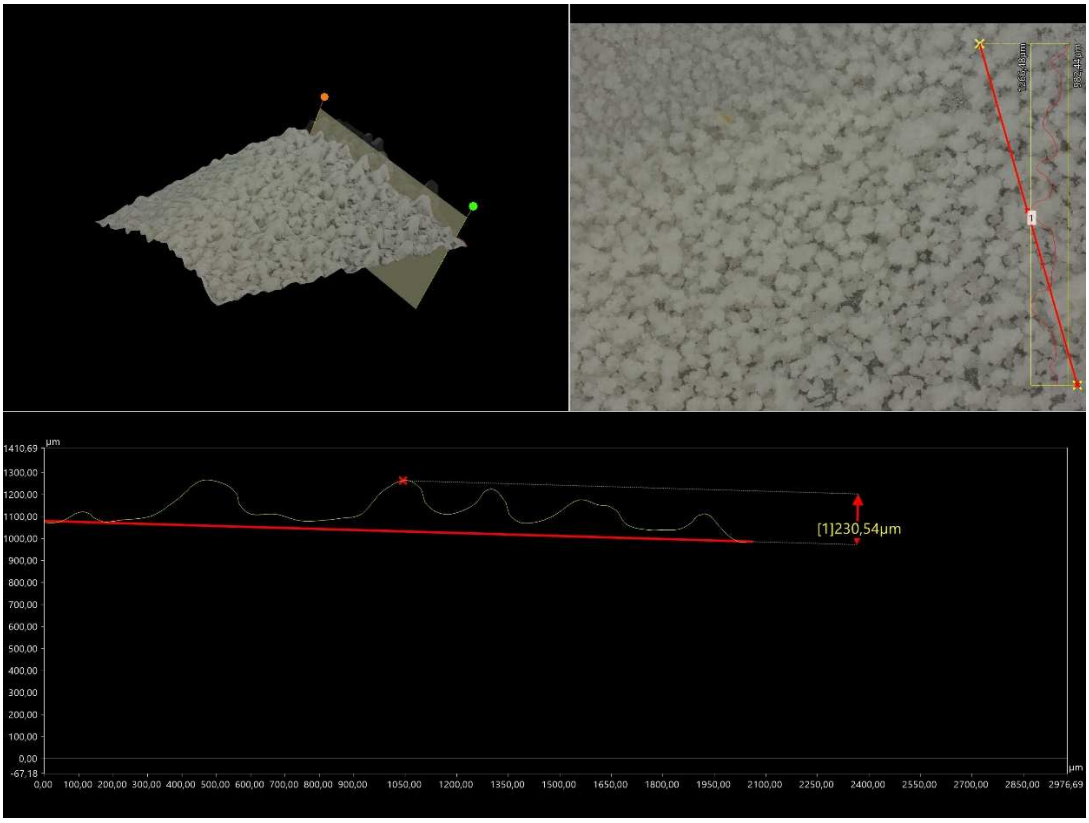

Figure 7: Results of digital microscope 3D - the thickness of the deposited scale in the inlet of the first cold compartment without treatment after 72 hours of heating, 50 °C, 100 $L.h^{-1}$

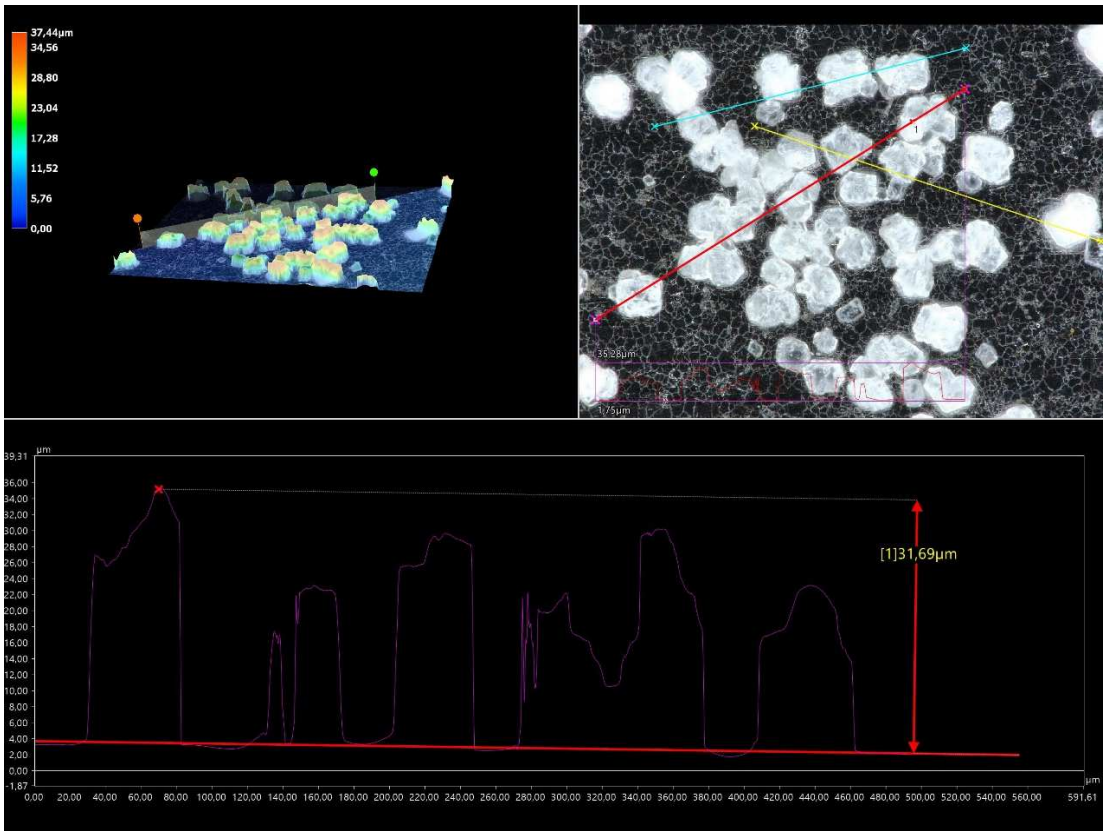

Figure 8: Results of digital microscope 3D - the thickness of the deposit at the outlet of the last cold compartment of the exchanger without treatment after 72 hours of heating, 50 °C, 100 L.h^{-1}

2.3.2 With ultrasonic treatment

In the presence of the ultrasonic transducer of medium power, and under the same operating conditions as before, a reduction in the thickness of the scale in all the compartments on the cold side is noted. In the first compartment, the maximum thickness of scale decreases from 230 µm to 8 µm. The same trend is observed for the last compartment, the analysis of the plates shows a reduction of the deposit thickness from 32 µm to 20 µm.

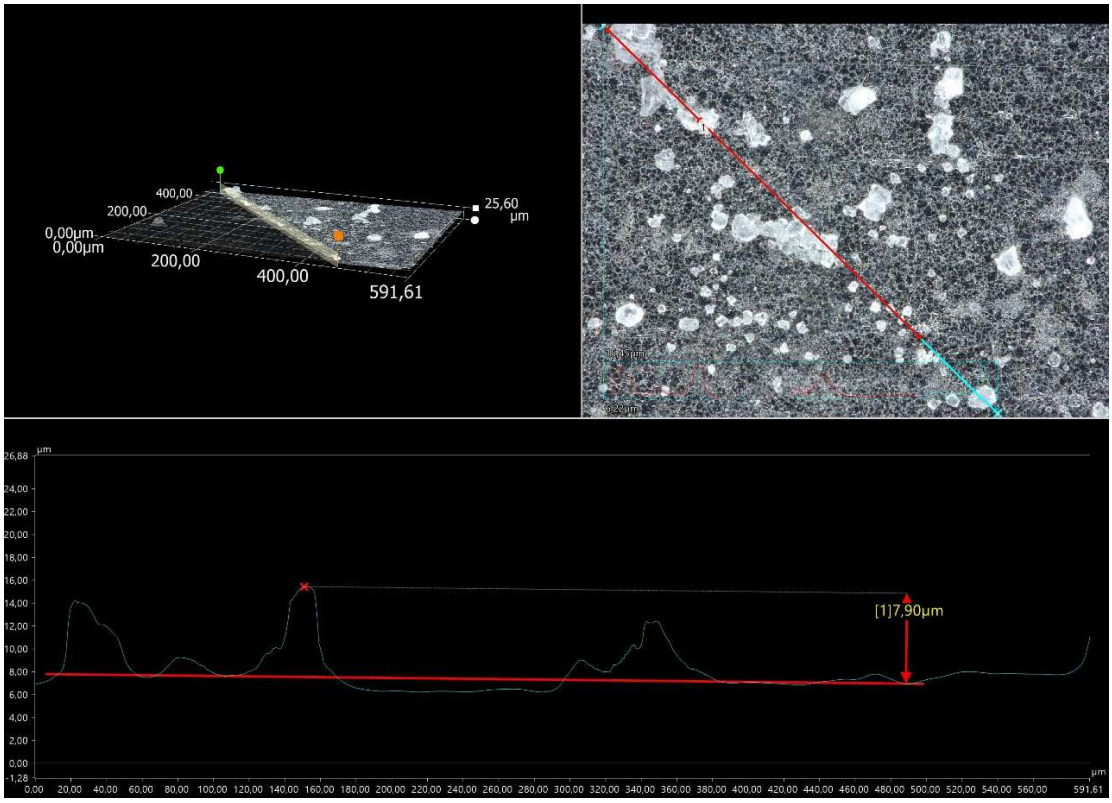

Figure 9: Results of digital microscope 3D - the thickness of the deposit at the inlet of the first cold compartment in the presence of the ultrasonic transducer after 72 hours of heating, 50 °C, 100 L.h^{-1}

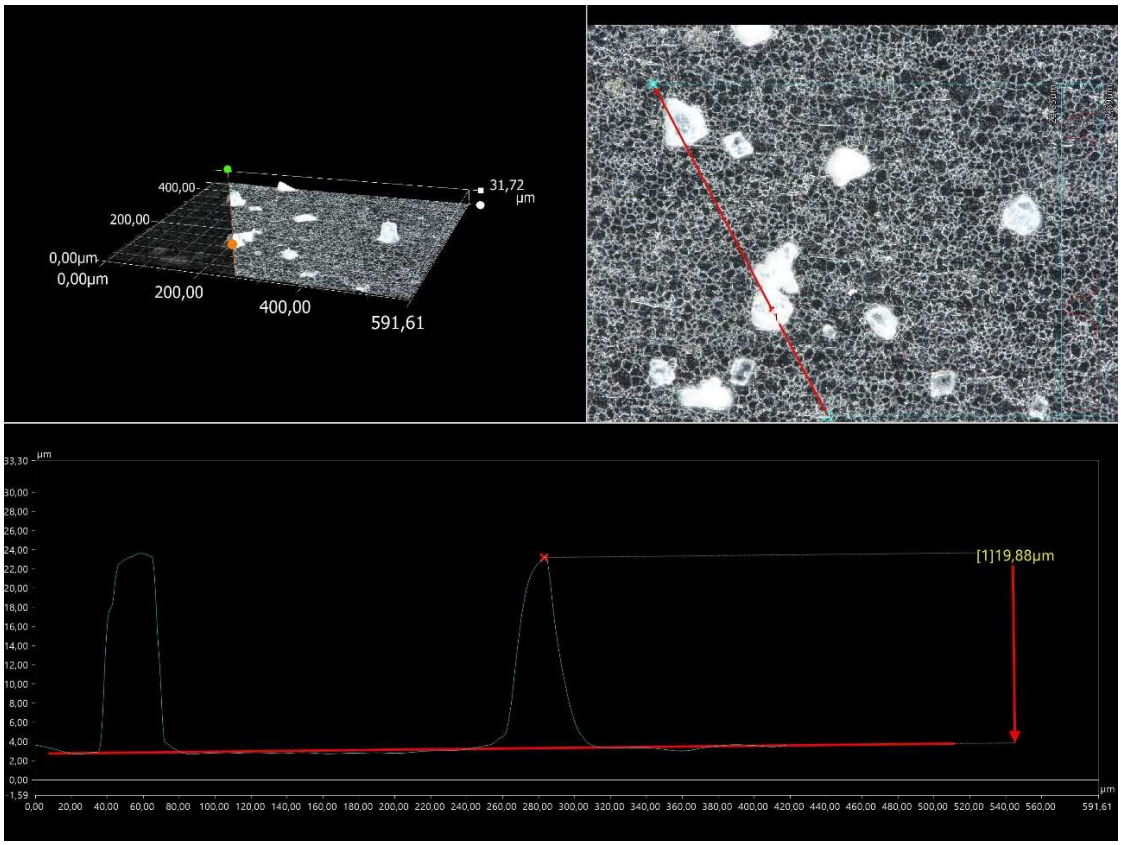

Figure 10: Results of digital microscope 3D - the thickness of deposit at the outlet of the last cold compartment of the exchanger with ultrasonic treatment after 72 hours of heating, 50 °C, 100 $L.h^{-1}$

Analysis of the plates with a 3D digital microscope shows that the surface of the 316L steel plates is not smooth, which raises questions about the formation of scale in the microporosity of the plates. Therefore, an analysis was performed with a confocal laser microscope to determine the surface roughness of the plates.

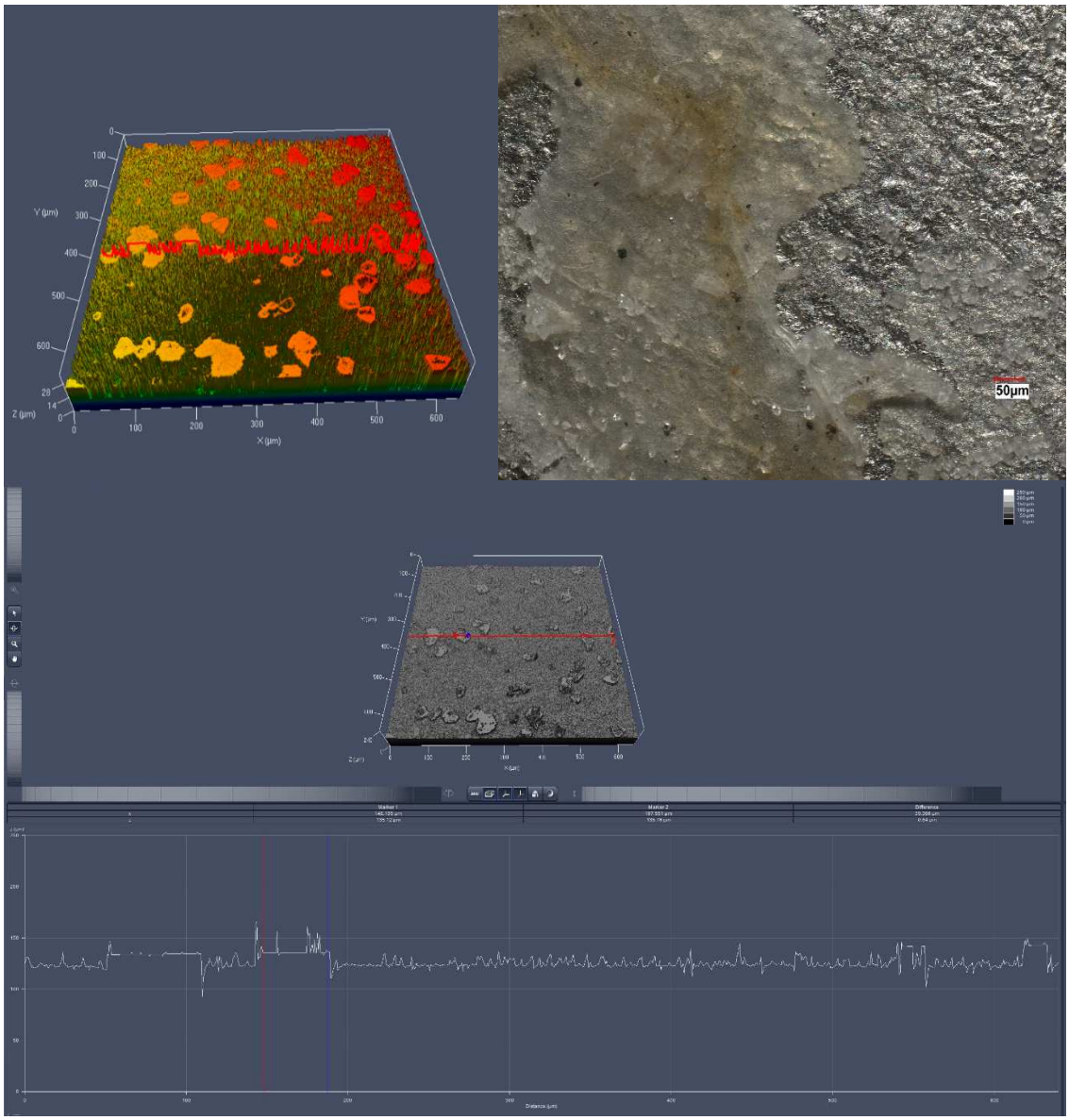

Figure 11: The surface of an exchanger plate observed with a 3D digital microscope and the 3D roughness analyzed with a confocal laser microscope

The analysis of the surface roughness shows that the value of the profile roughness determined during the measurement is 4.333 µm. The value of the surface roughness determined in the

measurement is 5.313 µm. Therefore, the size of the crystals formed on the surface is much larger than the microporosity of the surface.

The series of graphs presented in the figure above show that the crystals are not integrated into the internal structure of the plates.

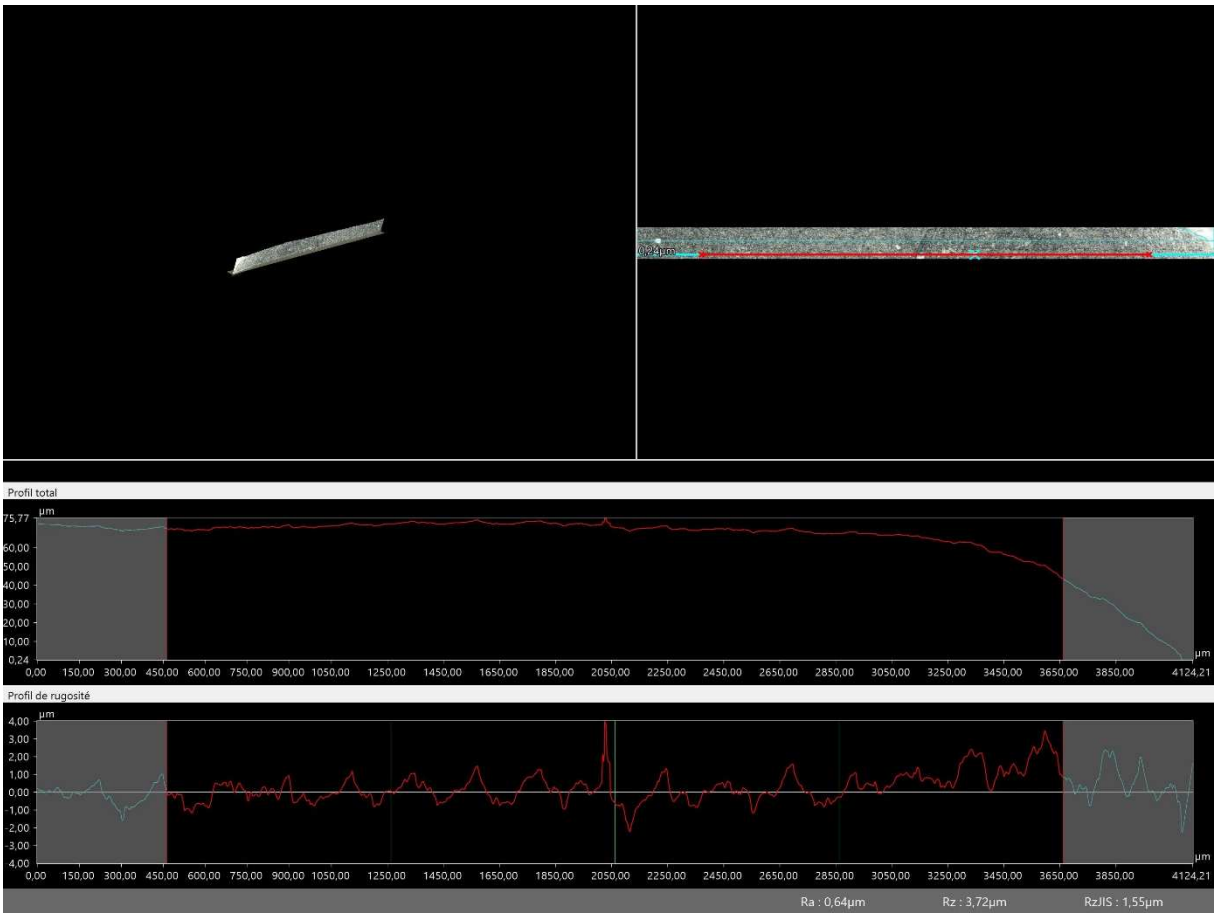

Figure 12: Results of digital microscope 3D - the surface roughness of a clean plate under a digital microscope.

2.1 Identification of the nature of formed solid

2.1.1 Raman spectrometer analysis

RAMAN spectroscopy has been applied to the study of calcium carbonate (Manel, 2019). This has allowed the characterization of the different forms of calcium carbonate, including amorphous calcium carbonate (Chao et al., 2014)

Among the most important parameters in the analysis of the mineral content of samples, the RAMAN "hit" count is essential, as the mineral proportions can be estimated based on the frequency of occurrence of the spectrum (Xi et al., 2018).

The main attraction of Raman spectroscopy in this case is that no sample preparation is required. The resulting deposit is usually a powder that can be simply deposited on a slide and then analyzed by the technique mentioned.

The RAMAN analysis was done 3 times for 3 trials performed under the same operating conditions. The spectra obtained for the different tests are identical, which indicates that the precipitation of the same polymorphic form is obtained in the 3 tests.

The RAMAN spectrum of the mineral deposit in the 1600 to 70 cm^{-1} region is shown in the following figure:

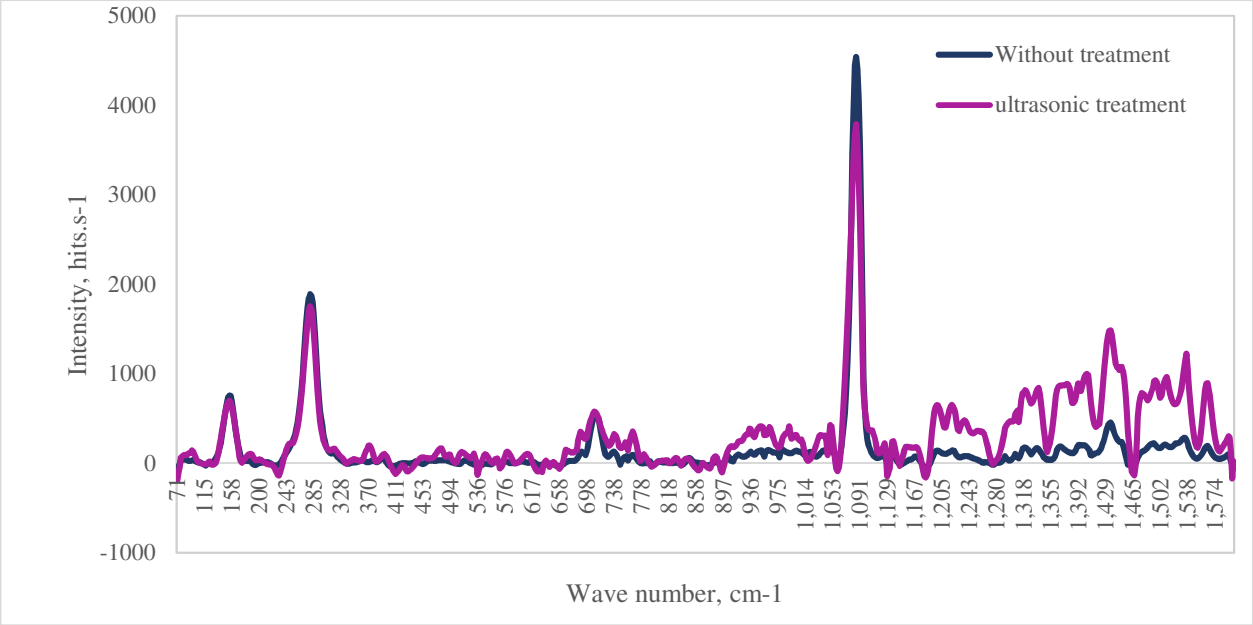

Figure 13**:** RAMAN spectrum of the scale formed on the inner surface of the tube at the outlet of the cold side exchanger, after 78 h ($[Ca^{2+}]_{initial}$ = 143.52 mg.L-1 ; $[CO_3^{2-}]_{initial}$ = 46.46 $mg.L^{-1}$; pH = 7.5, $[Ca^{2+}]_{final}$ = 66.54 $mg.L^{-1}$; $[CO_3^{2-}]_{final}$ = 21.09 $mg.L^{-1}$; 49 °C)

The theory of Junmin Sun and Zeguang Wu is based on the subdivision of the calcite spectrum into three sections (Sun et al., 2014):

- 1700-1200 cm^{-1}: attributed to the asymmetric stretching mode of CO_3^{2-}.
- 1200-600 cm^{-1}: due to the symmetrical stretching of CO_3^{2-}.

The appearance of a band at 1085.86 cm^{-1} with high intensity is characteristic of calcite (Sun et al., 2014)

There is also the appearance of a peak at 710.96 cm^{-1} (close to 715 cm^{-1}) which is also characteristic of calcite (El-Mofty et al., 2021) due to the symmetric deformation of CO_3^{2-}

(Sun et al., 2014).

Dolomite is characterized by the presence of the typical triplet bands in the region between 1069 and 1098 cm^{-1} (Sun et al., 2014),

- 100-500 cm^{-1}: due to the external vibration of CO_3^{2-}.

Two characteristic bands at 153.73 cm^{-1} and 279.68 cm^{-1} are also observed in the low wavenumber region, these are also characteristic waves of calcite that originate from the external vibration of the CO_3^{2-} group and involve rotational and translational oscillations of these groups (Sun et al., 2014).

2.1.2 Scanning Electron Microscope (SEM) Observation

SEM was used to analyze in detail the shape, size and degree of agglomeration of calcium carbonate crystals (Manel, 2019), and the chemical nature of the crystal by using the energy dispersive X-ray spectroscopy (EDXS) probe.

We observed the $CaCO_3$ powders obtained after 72 hours of heating with the JEOL Scanning Electron Microscope, JSM-6490-LV. In all the samples analyzed by SEM without ultrasonic treatment, calcium carbonate is present in the form of cubes which are characteristic of calcite crystals. In the photographs below, large agglomerates of mineralogically homogeneous calcite are observed.

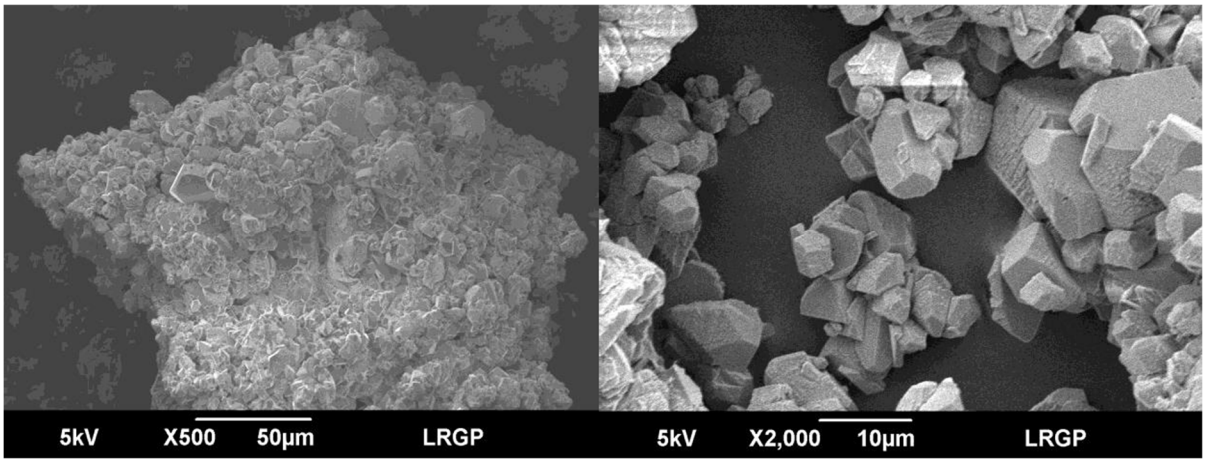

Figure 14: Results of scanning electron microscope analysis of the precipitates obtained after 72 hours of heating at 50 °C without treatment

To confirm this result, an EDXS analysis was performed to determine the atomic percentage of

Mg^{2+} and Ca^{2+}:

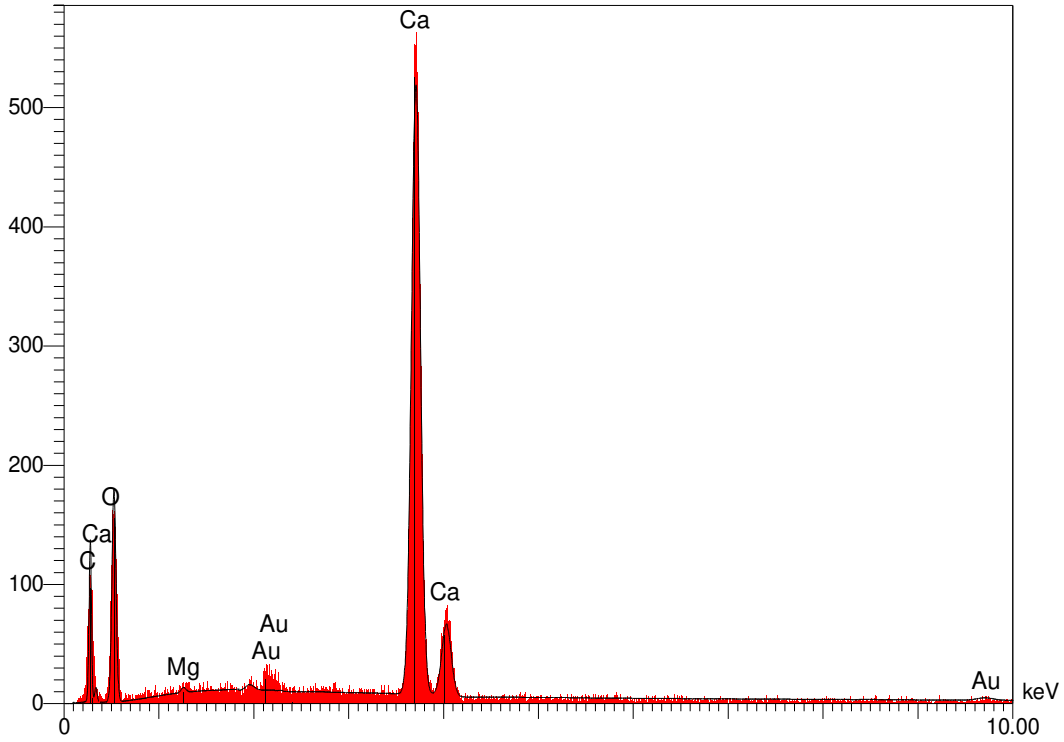

Figure 15: Results of energy dispersive X-ray spectroscopy analysis of crystals formed without treatment

The EDXS analysis shows the presence of Ca^{2+} with an atomic percentage of 17.43%, 100 times more than for Mg^{2+} (atomic percentage of 0.13%).

The gold peak is due to the plating of the samples.

Furthermore, a close examination of the high-resolution SEM imaging of the scaled surface in the presence of the transducer shows that the predominant form is calcite in the form of agglomerates.

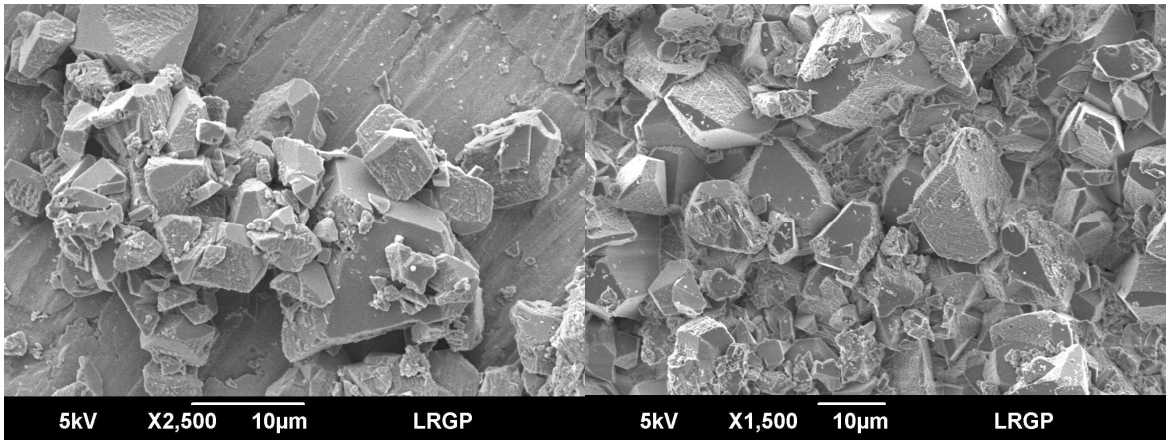

Figure 16: Results of scanning electron microscope analysis of crystals formed in the presence of ultrasonic treatment

EDXS was performed on the SEM image. The results show that the scale formed is predominantly $CaCO_3$.

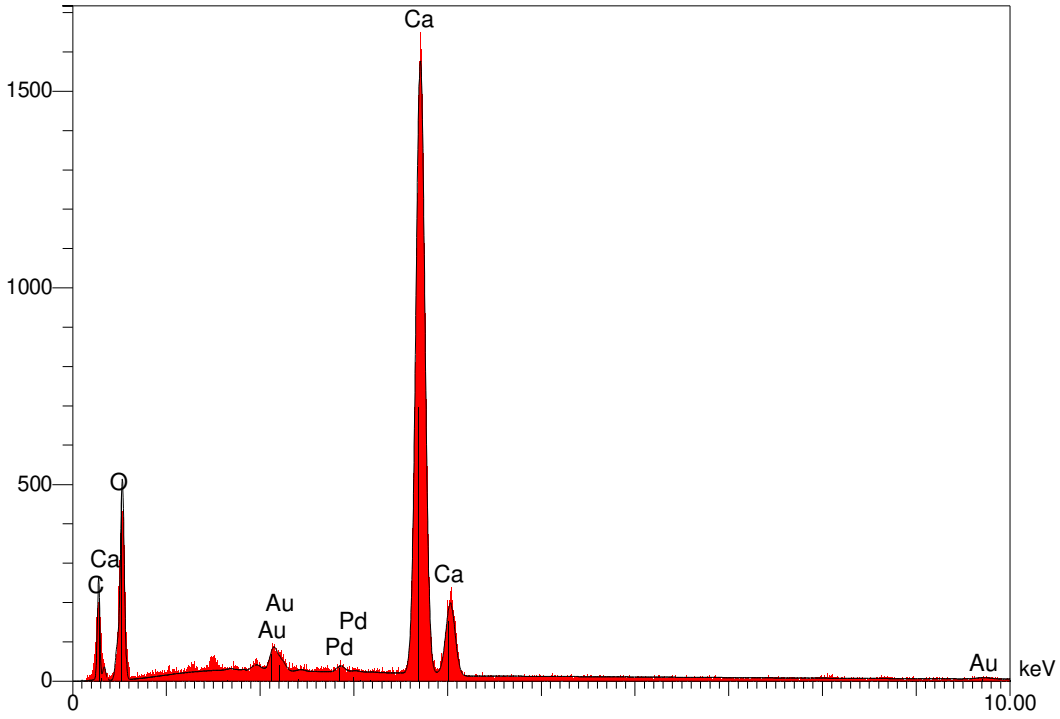

Figure 17: Results of energy dispersive X-ray spectroscopy of scale in the presence of ultrasonic treatment

As a result, the SEM and RAMAN results are consistent. The crystalline structure of calcite is similar in the different tests, both in the presence and absence of the ultrasonic transducer.

2.2 Analysis by laser granulometry

The particle size distribution was obtained by laser granulometry. The following figure shows the particle size distribution of the samples recovered at the end of each experiment.

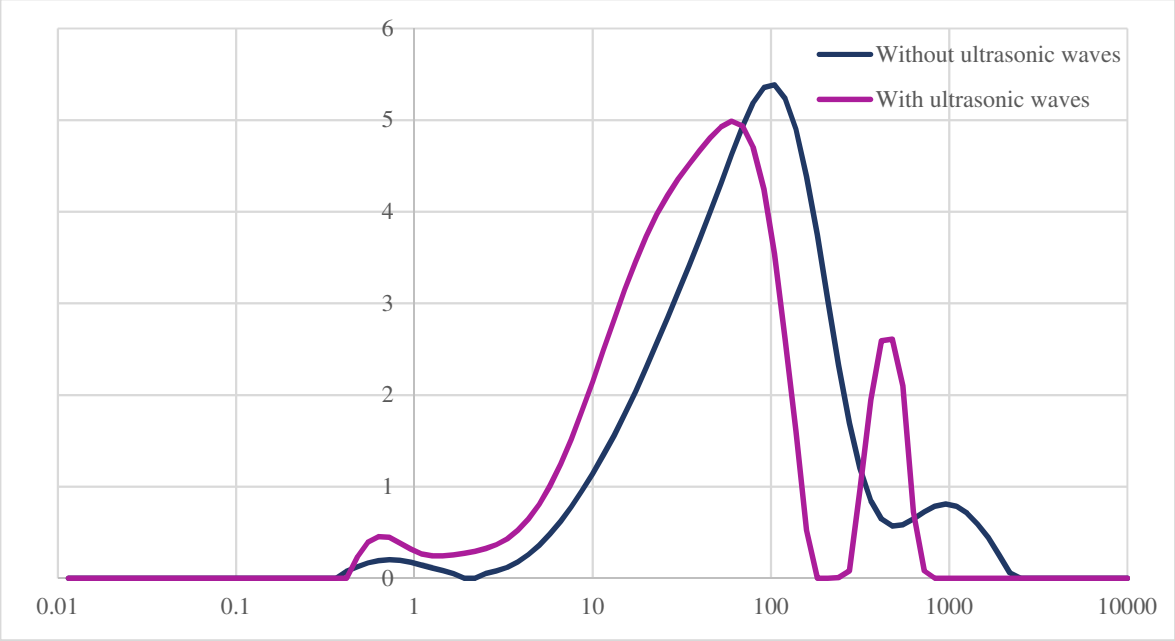

Figure 18: Particle distribution in the absence and presence of the ultrasonic treatment

In the absence of the ultrasonic treatment, the analyzed population is quasi-monomodal, with an average size of about 250 ± 10 µm. After the installation of the ultrasonic transducer at the outlet of the exchanger, a reduction in the size of the calcite crystals is observed. The particle size analysis indicates that the volume average diameter is about 80 ± 10 µm. A 68% reduction in crystal size is thus obtained.

2.3 Fraction of surface covered by tartar

A surface of 3.55 mm^2 was analyzed by 3D microscopy at the entrance of the first cold compartment without treatment. 78.2% of the surface is covered with calcite crystals.

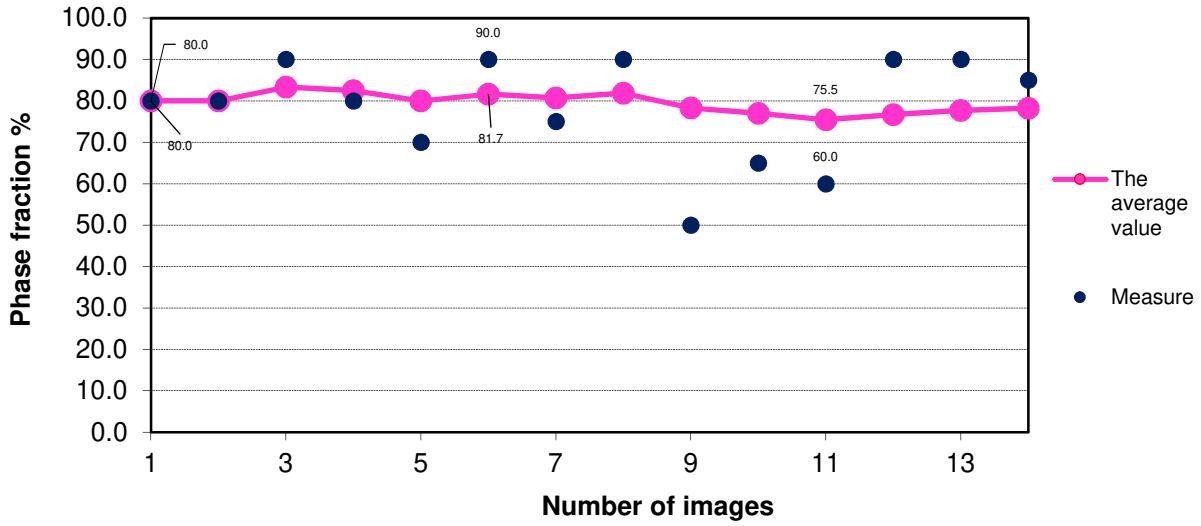

Figure 19: Analysis of the plates of the first compartment (cold circuit inlet) in the absence of the ultrasonic treatment under the 3D digital microscope

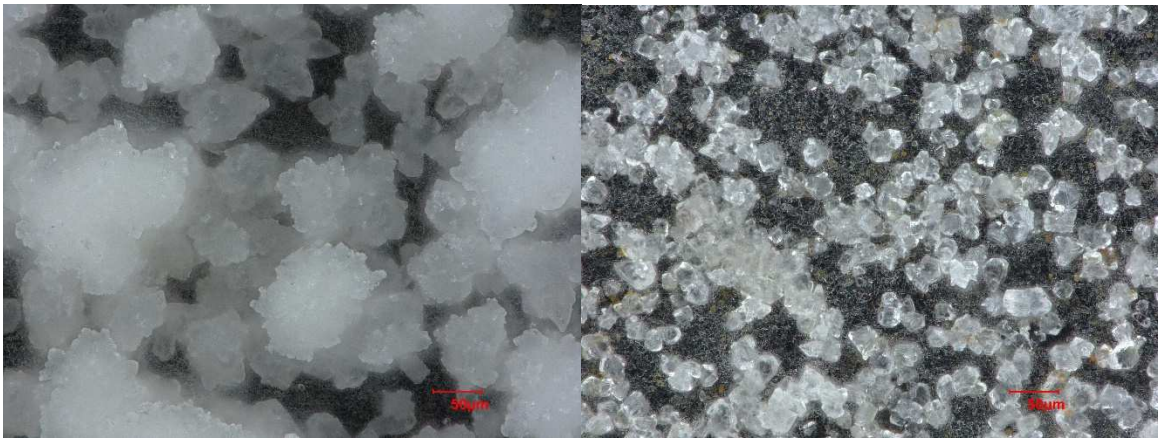

Figure 20: Most scaled and least scaled image of measurement session without ultrasonic treatment

In the presence of ultrasonic guided waves, only 6.8% of the surface is covered by crystals.

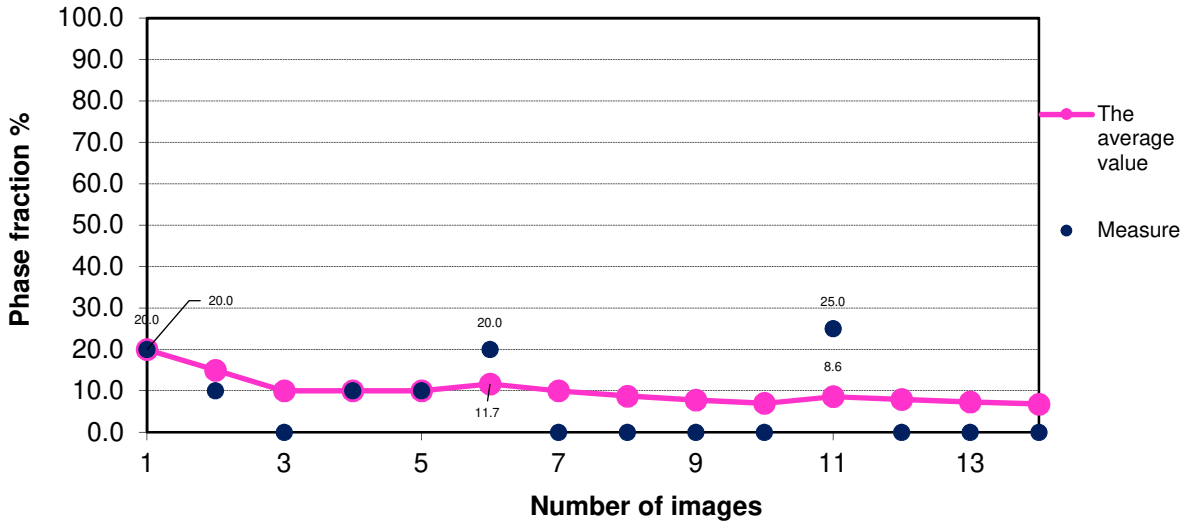

Figure 21: Analysis of the plates of the first compartment (cold circuit outlet) in the presence of the ultrasonic treatment with a 3D digital microscope

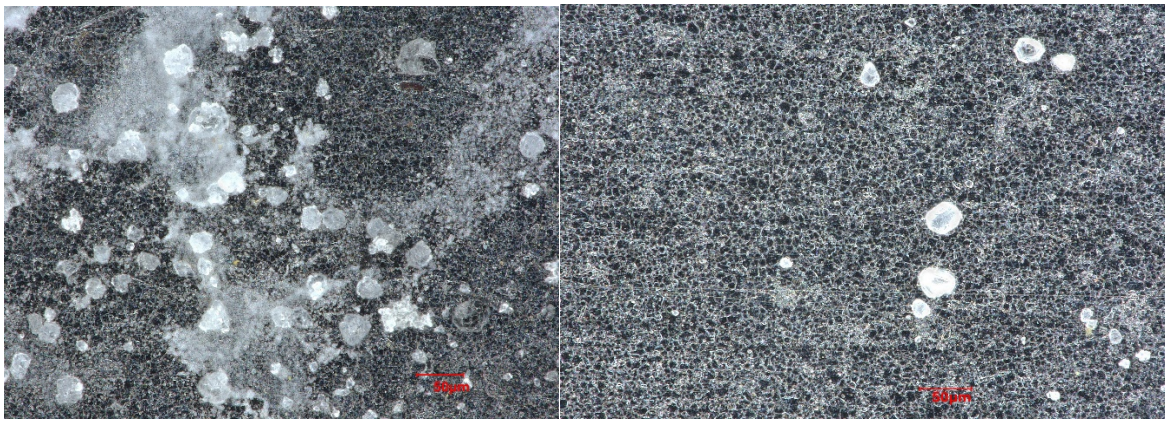

Figure 22: Most scaled and least scaled measurement session image in the presence of ultrasonic treatment

2.1 Distribution of calcium in different forms

The material balance is performed based on the ICP-OES results. The scale is dissolved in 5 L of 2% (vol) nitric acid, ħ _ This acid leaching releases the scale into the water. This acid leaching releases Ca^{2+} and Mg^{2+} ions in solution, which allows to estimate the amount of scale deposited in the cold compartment of the m $CaCO_3$_heat_exchanger. The monitoring of the ion concentrations in the scaling solution, at the beginning of the manipulation [$^{2+}$] , and at the end of the experiment, [$^{2+}$] , allows us to determine the distribution of calcium within the experimental device, whether it is in dissolved or precipitated form, in the exchanger and in the tank. The mass of precipitated calcium in the form of carbonate and remaining in the storage

tank, $_{3(\ )}$ is calculated according to the equations below.

$$n_{Ca^{2+},tank,i} = n_{Ca^{2+},tank,f} + n_{CaCO_{3(s)}heat\_exchanger} + n_{CaCO_{3(s)}tank}$$

$$\Leftrightarrow n_{CaCO_{3(s)}tank} = n_{Ca^{2+},tank,i} - n_{Ca^{2+},tank,f} - n_{CaCO_{3(s)}heat\_exchanger}$$

$$\Leftrightarrow m_{CaCO_{3(s)}tank} = M_{CaCO_3}\begin{pmatrix}[Ca^{2+}]_{tank,i}V_{tank} - [Ca^{2+}]_{tank,f}V_{tank} \\ -[Ca^{2+}]_{leaching_{sol}}V_{leaching_{sol}}\end{pmatrix}$$

Below, on an example, the distribution of dissolved calcium and precipitated calcium carbonate is presented. 4 typical experiments are presented in this paper, describing the system in its initial state in Ca^{2+} and its final state in Ca^{2+} / $CaCO_3$, in the presence and absence of ultrasound.

Table 3: Material balance of calcium forms (solid, dissolved) - T_f = 20 °C; T_c °C (50), flow rate 100 L.h^{-1}

Reference	***A***	***B***
Presence of US	No	Yes
$[Ca^{2+}]_{tank,i}$ *(mg/L)*	137,35	88,31
$[Ca^{2+}]_{tank,i}$ *(mmol/L)*	3,433	2,208
$n_{Ca^{2+}tank,i}$ *(mol)*	0,343	0,221
$[Ca^{2+}]_{tank,f}$ *(mg/L)*	68,44	36,13
$[Ca^{2+}]_{tank,f}$ *(mmol/L)*	1,711	0,903
$n_{Ca^{2+}tank,f}$ *(mol)*	0,171	0,90
$m_{CaCO_{3(s)}heat\_exchanger}$ *(g)*	4,79	1,12
$n_{CaCO_{3(s)}heat\_exchanger}$ *(mol)*	0,048	0,012
$m_{CaCO_{3(s)}tank}$ *(g)*	12,44	11,93
$n_{CaCO_{3(s)}tank}$ *(mol)*	0,124	0,119

With,

[$^{2+}$] , Initial concentration in mg/L of Ca^{2+}.

[$^{2+}$] , Final Ca^{2+} concentration in mg/L

- **Test A**: Monitoring of scale formation in the absence of the 35-50 kHz transducer.

$[Ca^{2+}]_{Initial}$ = 137.35 mg/L, or 34.34 g $CaCO_3$ equivalent $[Ca^{2+}]_{Final}$ = 68.44 mg/L, or 16.52 g $CaCO_3$ equivalent CaCO3 deposited in the exchanger = **4.79** g $CaCO_3$ CaCO3 deposited in the circuit =12.44 g $CaCO_3$

- **Test B**: Monitoring of scale formation in the presence of the 35-50 kHz transducer.

$[Ca^{2+}]_{Initial}$ = 88.31 mg/L (22.07 g $CaCO_3$ eq.) $[Ca^{2+}]_{final}$ = 36.13 mg/L (9.03 g eq. $CaCO_3$) $CaCO_3$ deposited in the exchanger = **1.12 g** $CaCO_3$ deposited in the circuit = 11.92 g

- **Test C**: Disassembly of the exchanger without the 35-50 kHz transducer.

$[Ca^{2+}]_{Initial}$ = 157.84 mg/L (39.46 g eq. $CaCO_3$)

$[Ca^{2+}]_{Final}$ = 74.19 mg/L (18.54 g eq. $CaCO_3$)

$CaCO_3$ deposited in the circuit + $CaCO_3$ deposited in the exchanger (distributed over all the plates) = 20.92 g

- **Test D**: Disassembly of the exchanger in the presence of the 35-50 kHz transducer.

$[Ca^{2+}]_{Initial}$ = 92.11 mg/L (23.02 g eq. $CaCO_3$)

$[Ca^{2+}]_{Final}$ = 66.11 mg/L (16.52 g eq. $CaCO_3$)

CaCO3 deposited in the circuit + $CaCO_3$ deposited in the exchanger (distributed over all the plates) = 6.5 g

Thus, after three days, calcium is present in dissolved form as well as in precipitated form. Note that most of the solid calcium carbonate is present in the storage tank and not on the walls of the exchanger.

Conclusion

A pilot heat exchanger was designed and developed to experimentally study the scaling phenomenon in the presence or absence of ultrasonic guide waves. The deposit of calcium carbonate precipitated inside the heat exchanger without ultrasonic treatment is of the order of 4.8 ± 0.9 grams/day/m^2, it consists of calcite agglomerates with a mass average size of 250 ± 10 µm.

A low power (medium power) 35-50 kHz ultrasonic transducer is used to limit scale formation. Experiments show a clear reduction in deposits, of the order of 76 %, with only a deposit of 0.98

± 0.5 grams/day/m2. This deposit is made up of calcite agglomerates of average size 80 ± 10 µm.

RAMAN spectroscopy and SEM imaging show that in all experiments it is the formation of calcite that is observed. Therefore, the ultrasonic treatment has no influence on the polymorphism of the precipitated calcium carbonate.

Analysis of the plates with a 3D microscope shows that the distribution of scale on a plate is not homogeneous. Therefore, it is necessary to carry out a more detailed study of the distribution of scale as a function of temperature and fluid flow in order to detect areas susceptible to scale formation.

The concept of ultrasonic treatment therefore gives very encouraging results, with a clear reduction in the amount of tartar formed, without however totally preventing its formation.

Further experiments will be considered in the presence of two transducers of different frequency to study the influence of the combination of multi-frequency transducers with the scanning technique on the formation of mineral scale.

Author's statements

This study is part of the ExUS project, directed by Dr. Hervé MUHR as thesis director. Dr. Marie LE PAGE MOSTEFA is co-director of the thesis. Mrs. Nihad KAMAR built the heat exchanger pilot and performed the experimental measurements. Mr. Pierre-Olivier JOST is the project leader.

- Author Information:

- Dr. Hervé MUHR: University of Lorraine, Reactions and Process Engineering Laboratory (LRGP) UMR 7274 CNRS, 1 rue Grandville BP20451, 54001 Nancy, France.
- Dr. Marie LE PAGE MOSTEFA: University of Lorraine, Reactions and Process Engineering Laboratory (LRGP) UMR 7274 CNRS, 1 rue Grandville BP20451, 54001 Nancy, France.
- Nihad KAMAR: University of Lorraine, Reactions and Process Engineering Laboratory (LRGP) UMR 7274 CNRS, 1 rue Grandville BP20451, 54001 Nancy, France. nihad.kamar@univ-lorraine.fr
- Pierre-Olivier JOST: Sofchem, 9 rue du Gué, 92500 Rueil Malmaison, France.

Financial Statement

The authors acknowledge the financial support of the Grand EST region, BPI France bank in the framework of the ExUS project.

This contribution is the result of the implementation of the project: Control of fouling by the use of ultrasonic guided waves associated with the heterodyne effect of multiple frequencies, supported by the ERDF funded development.

Acknowledgements

The authors thank the Grand-Est region, BPI France and the European Regional

Development Fund for their financial support.

Declaration of competing interests

The authors declare that they have no known competing financial interests or personal relationships that might appear to influence the work reported in this article.

References

Alsemgeest, J., Auqué, L.F., Gimeno, M.J., 2021. Verification and comparison of two thermodynamic databases through conversion to PHREEQC and multicomponent geothermometrical calculations. Geothermics 91. https://doi.org/10.1016/j.geothermics.2020.102036

Bezák, T., Kusý, M., Eliáš, M., Kopček, M., 2013. Surface roughness determination using laser scanning confocal microscope zeiss LSM 700. Met. 2013 - 22nd Int. Conf. Metall. Mater. Conf. Proc. 947-952.

Chao, Y., Horner, O., Hui, F., Lédion, J., Perrot, H., Chao, Y., Horner, O., Hui, F., Lédion, J., Perrot, H., 2014. Direct detection of calcium carbonate scaling via a pre-calcified sensitive area of a quartz crystal microbalance To cite this version : HAL Id : hal-01079703 Direct detection of Calcium Carbonate Scaling via a Pre-Calcified Sensitive Area of a Quartz Cry.

Corrieu, G., Lalande, M., Ferret, R., 1986. On-line measurement of fouling and cleaning of an industrial UHT sterilizer. J. Food Eng. 5, 231-248. https://doi.org/10.1016/0260-8774(86)90027-0

De, D., Grenoble, D.E., Legay, M., 2012. Intensification of ultrasonic heat transfer processes , towards a new type of heat exchanger : the vibrating exchanger.

Deeley, C.M., Spragg, R.A., Threlfall, T.L., 1991. A comparison of Fourier transform infrared and near-infrared Fourier transform Raman spectroscopy for quantitative measurements: An application in polymorphism. Spectrochim. Acta Part A Mol. Spectrosc. 47, 1217-1223. https://doi.org/10.1016/0584-8539(91)80208-Z

El-Mofty, S.E., Patra, P., El-Midany, A.A., Somasundaran, P., 2021. Dissolved Ca2+ ions adsorption and speciation at calcite-water interfaces: Thermodynamics and spectroscopic studies. Sep. Purif. Technol. 257, 117834. https://doi.org/10.1016/j.seppur.2020.117834

Eldeeb, R., Aute, V., Radermacher, R., 2016. A survey of correlations for heat transfer and pressure drop for evaporation and condensation in plate heat exchangers. Int. J. Refrig. 65, 12- 26. https://doi.org/10.1016/j.ijrefrig.2015.11.013

Habibi, H., Gan, T.-H., Legg, M., Carellan, I., Kappatos, V., Tzitzilonis, V., Selcuk, C.,

2020. an Acoustic Antifouling Study in Sea Environment for Ship Hulls Using Ultrasonic Guided Waves. Int. J. Eng. Technol. Manag. Res. 3, 14-30.

https://doi.org/10.29121/ijetmr.v3.i4.2016.59

Manel, G., 2019. Protection of carbon steel against scaling by a non-toxic polymer treatment and doping with copper and zinc cations. SORBONNE UNIVERSITY TUNIS EL MANAR.

Mathieu, L., Keraval, A., Block, J., Mougel, J.-F., Mathieu, D., Jost, J., Machicado, S., n.d. Assessment of low-power ultrasound device on biofilm formation and carbonate deposition in heat exchanger: a lab study CleanUS-EU / FEDER-FSE Lorraine et Massif des Vosges, et Région Grand Est.

Monti, M., 2012. Basic confocal microscopy. Eur. J. Histochem. 56, 3. https://doi.org/10.4081/ejh.2012.br3

Parkhurst, D., Appelo, C.A.J., 1999. User's guide to PHREEQC (Version 2) - A computer program for speciation, batch-reaction, one-dimensional transport, and inverse geochemical calculations, Water-Resources Investigations Report 99-4259 U.S. Geological Survey, Denver, Colorado, 1999. 4259.

Parkhurst, D.L., 1995. ADVECTIVE-TRANSPORT, AND INVERSE GEOCHEMICAL

CALCULATIONS Water-Resources Investigations Report 95-4227.

Sun, J., Wu, Z., Cheng, H., Zhang, Z., Frost, R.L., 2014. A Raman spectroscopic comparison of calcite and dolomite. Spectrochim. Acta - Part A Mol. Biomol. Spectrosc. 117, 158-162. https://doi.org/10.1016/j.saa.2013.08.014

Taylor, R.J., Richardson, L.B., 1982. Ultrasonics As an Alternative To Chlorine 3, 295-

297. Thyne, G.D., 2017. PHREEQC 2007 Manual for Short Course.

Xi, S., Zhang, X., Du, Z., Li, L., Wang, B., Luan, Z., 2018. Journal of Asian Earth Sciences Laser Raman detection of authigenic carbonates from cold seeps at the Formosa Ridge and east of the Pear River Mouth Basin in the South China. J. Asian Earth Sci. 168, 207-224. https://doi.org/10.1016/j.jseaes.2018.01.023